DRAFT VERSION APRIL 2, 2020
Preprint typeset using LaTeX style emulateapj v. 01/23/15

EFFECT OF ACTIVE GALACTIC NUCLEI THERMAL HEATING WITH RADIAL DEPENDENCE ON THERMAL STABILITY OF SIMULATED GALAXY CLUSTERS

FORREST W. GLINES [1,2,4], BRIAN W. O'SHEA [1,2,3], G. MARK VOIT[1]
[1]Department of Physics and Astronomy, Michigan State University, East Lansing, MI 48824, USA
[2]Department of Computational Mathematics, Science, and Engineering, Michigan State University, East Lansing, MI 48824, USA
[3]National Superconducting Cyclotron Laboratory, Michigan State University, East Lansing, MI 48824, USA and
[4]glinesfo@msu.edu

Draft version April 2, 2020

ABSTRACT

Observations since the 1970's have revealed the existence of cool-core (CC) clusters, which are galaxy clusters with a central cooling time much shorter than the age of the universe. Both observations and theory suggest that the ambient gas at the centers of galaxy clusters is thermally regulated by a central heating mechanism that suppresses condensation (most likely an active galactic nucleus, or AGN). Previous analytical work has suggested specific configurations of heating kernels that may result in thermal balance and a steady state. To test this hypothesis, we simulated idealized galaxy clusters using the ENZO cosmology code with a spatial heat-input kernel meant to mimic feedback from a central AGN. Thermal heating as a function of radius was injected according to a range of kernels, with global thermal balance enforced at all times. We compare our simulation results with observed entropy profiles from the ACCEPT cluster dataset. Although some heating kernels produced thermally steady galaxy clusters, no kernel was able to produce a steady cluster with a central entropy as low as the central entropies typically observed among CC clusters. The general behavior of the simulations depended on the amount of heating in the inner 10 kpc, with low central heating leading to central cooling catastrophes, high central heating creating a central convective zone with an inverted entropy gradient, and intermediate heating leading to a flat but elevated entropy core. The simulated clusters enter an unsteady multiphase state on a timescale proportional to the square of the cooling time of the lowest entropy gas in the simulation, with centrally concentrated heating resulting in a steady state lasting for a longer period of time.

1. INTRODUCTION

Cool-core (CC) clusters have X-ray surface brightness profiles with sharp central peaks produced by substantial radiative losses of thermal energy from gas within the central few tens of kpc. Given the observed rates of energy loss, CC clusters should be capable of radiating away their central thermal energy in less than 1 Gyr. If uncompensated, such a rapid cooling rate would lead to a cooling catastrophe in which multiphase condensation of ambient gas into cold clouds fuels star formation rates much greater than those observed. However, CC clusters are generally not observed to experience such dramatic cooling catastrophes (McDonald et al. 2019). They apparently remain close to thermal balance for billions of years and are common, representing about half of all galaxy clusters at the present time. Consequently, some mechanism must be counteracting central radiative cooling, and active galactic nuclei (AGN) are currently believed to be the responsible energy sources (Fabian et al. 2000; McNamara et al. 2000; Fabian et al. 2006; McNamara & Nulsen 2007; Panagoulia et al. 2014; Gaspari 2016).

While many other heat sources have been explored, including galaxy cluster mergers (Roettiger et al. 1997; Gómez et al. 2002; ZuHone et al. 2010), supernovae (Ciotti & Ostriker 1997; Wu et al. 1998; Voit & Bryan 2001; Domainko et al. 2004; Short et al. 2013), thermal conduction (Chandran & Cowley 1998; Narayan & Medvedev 2001; Malyshkin & Kulsrud 2001; Voigt et al. 2002; Jubelgas et al. 2004; Brüggen 2003a; Smith et al. 2013), gravitational heating (Khosroshahi et al. 2004; Dekel & Birnboim 2007, 2008), and gas sloshing (Ritchie & Thomas 2002; Markevitch et al. 2001; ZuHone et al. 2010), most either do not provide enough heat to offset the observed cooling or do not adjust to the radiative cooling rate on a short enough time scale. Core cooling times in many CC clusters fall under 1 Gyr and well under the lifetimes of these clusters (Cavagnolo et al. 2009; Pratt et al. 2009), suggesting that any heating mechanism coupled to cooling must react on shorter timescales. The gas accretion rate onto the central supermassive black hole (SMBH) would therefore need to couple to the radiative cooling rate with a lag time no greater than several hundred Myr.

Heating by a central AGN was explored numerically as early as Tabor & Binney (1993) and Binney & Tabor (1995). More recently, Sijacki et al. (2007), Gaspari et al. (2011), Li et al. (2015), Meece et al. (2017), Prasad et al. (2015, 2017, 2018), and many others (Fabjan et al. 2010; Dubois et al. 2010; Short et al. 2013; Yang & Reynolds 2016) have demonstrated in hydrodynamic simulations of idealized galaxy clusters that AGN can plausibly regulate the high cooling rate in CC clusters. Simulated AGN self-regulate by coupling feedback energy output to the ambient gas density or cold-gas accretion rate around the AGN and inject that energy through either thermal deposition around the AGN or bipolar outflows from the AGN or a combination of the two. In addition to regulating the cooling rate and the condensation of cold gas clouds within the cluster, some of these AGN simulations produce temperature, density, and entropy profiles that resemble observations, including the multiphase cores observed in the central 100 kpc of galaxy clusters (Gaspari et al. 2012b; Meece et al. 2017; Prasad et al. 2018).

The simulations that most successfully resemble observations rely on cold-gas accretion to fuel the AGN and bipolar outflows to distribute the feedback energy (Voit et al. 2017; Gaspari et al. 2017; Gaspari & Sądowski 2017; Meece et al. 2017). Ambient gas at the center of the system is nearly isen-

tropic and therefore convectively unstable, resulting in the formation of a complex multiphase medium in which cold clumps of gas condense out of the ambient gas and precipitate onto the black hole. As the precipitation increases, so does the output of feedback energy, which raises the central cooling time and ultimately reduces the rate of precipitation. The resulting coupling suspends the ambient medium in a transitional state on the verge of a cooling catastrophe. Condensation outside of the isentropic center is marginally suppressed by buoyancy, and gas lifted out of the center by bipolar jets and buoyant bubbles forms multiphase filaments (Revaz et al. 2008; McDonald et al. 2010; Russell et al. 2016, 2017). However, even these idealized simulations do not track all of the physical processes that might be transporting and thermalizing AGN feedback energy, which range from turbulent heat diffusion (Ruszkowski & Oh 2011; Zhuravleva et al. 2014), viscous dissipation of waves generated by the AGN (Ruszkowski et al. 2004), and cosmic rays created by the AGN heating the plasma via small scale fluid instabilities (Böehringer & Morfill 1988; Loewenstein et al. 1991; Rephaeli & Silk 1995; Colafrancesco et al. 2004; Pfrommer et al. 2007; Jubelgas et al. 2008).

Incorporating all of these mechanisms and processes into a cosmological simulation of galaxy cluster formation is currently prohibitively complex. Typically, the minimum spatial resolution in simulations modeling hot jets that interact with the intracluster medium is 200 pc, with a resolution of at least 500 pc needed for convergence (Meece et al. 2017; Li et al. 2015). These resolution constraints are not feasible for large cosmological simulations, because the computational effort needed to model these AGN jets exerts unacceptable drag on the evolution of the entire system. Therefore, simplified AGN feedback prescriptions are needed in order to model AGN feedback in cosmological simulations while maintaining reasonable runtimes.

The results we present here emerged from an effort to develop a simple AGN feedback model that would remain thermally steady in a configuration similar to observed CC clusters. We sought a mechanism that would satisfy three criteria:

1. CC clusters balanced by AGN feedback should remain nearly thermally steady, meaning that they should not undergo a cooling catastrophe for several billion years.

2. The central entropy of such a CC cluster should not exceed observed values.

3. Numerical evolution of a CC cluster and its compensating AGN feedback should not require high resolution, small time steps, or otherwise time consuming computational tasks.

The first criterion requires the AGN feedback model to prevent a cooling catastrophe. Sufficient energy feedback to the cooling gas is needed from the AGN to prevent runaway overcooling. This state of balance can be difficult in a system with a centrally flattened entropy profile because buoyancy is then unable to suppress the runaway thermal instability that results in multiphase condensation. However, observations show that CC clusters can remain remarkably close to a cooling catastrophe without producing an overabundance of cold gas and young stars.

The second criterion requires that the AGN not provide too much feedback in the central region, which would raise or invert the flattened entropy profile. Such centrally concentrated AGN feedback can produce both non-cool core (NCC) clusters or observationally unreasonable galaxy clusters with large central entropy peaks. Satisfying both this criterion and the first one proved to be difficult.

Our attempts to satisfy the third criterion simultaneously with the other two were the main motivator for this paper. Tracking the rapid formation of a complex multiphase medium approaching a cooling catastrophe requires high resolution and small time steps. Furthermore, if the energy output from the AGN feedback model is linked to condensation of cold clouds, the approach of a cooling catastrophe leads directly to rapid central heating, which also raises the computational requirements.

To search for an adequate and numerically simple AGN feedback mechanism, we investigated a radial power-law distribution of thermal-only AGN feedback, with the total heating feedback set equal to the total cooling within the galaxy cluster. This heating kernel model abstracts the thermalization of more complex AGN feedback mechanisms into heat deposited radially. Depositing heat into the gas according to a kernel that depends only on radius is numerically simple and is efficient to incorporate into cosmological simulations. As long as the feedback can maintain a thermally steady cluster and prevent overcooling, high resolution is not needed. In order to create a tunable model, we also modified the radial power-law with an inner truncation radius to limit central feedback and an outer exponential cutoff radius to constrain the bulk of the AGN heating to gas with shorter and more relevant cooling times. With these additional parameters, we have a numerically simple but tunable model to search for an adequate AGN feedback model.

Section 2 discuses the simulation setup and AGN feedback prescription and heating kernel in detail. Section 3 shows simulation results, describing in detail the results of three heating kernels that broadly represent the whole set of simulations, and examining the impact of different heating kernel parameters. Section 4 discusses the adequacy of the heating kernels tested, the robustness of the AGN feedback model, and possible implications from these simulations. Lastly, Section 5 summarizes the results and conclusions of this work.

2. METHODOLOGY

2.1. *Simulation Setup*

We ran several simulations of idealized galaxy clusters with a simplified AGN heating model using the hydrodynamics code ENZO (Bryan et al. 2014).

We used initial conditions approximating the Perseus Cluster, following the approach from Li & Bryan (2012) and Meece et al. (2017). The ICM begins as a hydrostatic sphere of gas in a fixed gravitational potential.

The gravitational potential has two components: a dark matter halo profile and a BCG with a mass profile with parameters chosen to match the Perseus cluster. The dark matter follows the NFW profile (Navarro et al. 1997), using $M_{200} = 8.5 \times 10^{14} M_\odot$ for the mass within the virial radius and a concentration parameter $c = 6.81$. The dark matter density from the NFW profile takes the form

$$\rho^{\rm NFW}(r) = \frac{\rho_0^{\rm NFW}}{(r/R_s)\left(1+\frac{r}{R_s}\right)^2} \tag{1}$$

where the scale density $\rho_0^{\rm NFW}$ is defined by

$$\rho_0^{\rm NFW} = \frac{200}{3}\rho_c \frac{c^3}{\ln(1+c) - c/(1+c)}, \quad (2)$$

and the scale radius R_s can be found from

$$M_{200} = 4\pi\rho_0^{\rm NFW} R_s^3 \left[\ln(1+c) - c/(1+c)\right]. \quad (3)$$

The BCG mass profile, following Meece et al. (2017), has the form

$$M_*(r) = M_4 \left[\frac{2^{-\beta_*}}{\left(r/4\text{ kpc}\right)^{-\alpha_*}\left(1+r/4\text{ kpc}\right)^{\alpha_*-\beta_*}}\right], \quad (4)$$

where $M_4 = 7.5\times10^{10} M_\odot$ is the stellar mass within 4kpc and $\alpha_* = 0.1$ and $\beta_* = 1.43$ are constraints.[1]

The initial pressure was computed from the temperature and density assuming an ideal gas with $\gamma = 5/3$ in hydrostatic equilibrium with the gravitational potential. Cosmological expansion is neglected in these simulations. We used a vanilla ΛCDM model to get the virial mass of the NFW halo and to set its gas temperature. We set redshift $z = 0$ at initialization with $\Omega_M = 0.3$, $\Omega_\Lambda = 0.7$, and $H_0 = 70$ km s^{-1}. We note that the precise details of the cosmological model do not impact the results presented in later sections of this paper, which pertain to baryonic physics in the cluster core.

The entropy profile of the gas, using the form

$$K \equiv \frac{k_b T}{n_e^{2/3}} \quad (5)$$

for the specific entropy, where k_b is Boltzmann's constant, T is the temperature, and n_e is the electron density, was initialized to a power law

$$K(r) = K_0 + K_{100}\left(r/100\text{ kpc}\right)^{\alpha_K}, \quad (6)$$

following the power law fits used in the ACCEPT database (Cavagnolo et al. 2009). Here, r is the radius from the cluster center and $K_0 = 19.38$ keV cm^2, $K_{100} = 119.87$ keV cm^2, and $\alpha_K = 1.74$ are fitting parameters corresponding to the core entropy, entropy slope and exponential increase, chosen to approximate the Perseus Cluster.

The simulations were run in a cubic volume with side length of 3.2 Mpc, with 64^3 cells in the base grid of the AMR hierarchy and a maximum of 8 levels of refinement, making the resolution of the finest cells approximately 195 pc. The mesh was refined based on the magnitude of gradients in fluid quantities and high baryon density. Additionally, a cubic grid with side length 4 kpc was centered on the AGN and was fixed at the maximum level of refinement with 195 pc resolution.

Each simulation was allowed to run for 16 Gyr or until excessive AGN feedback during a cooling catastrophe either created unphysical cell values or led to intractably small timesteps (see Section 4.2.) To give context to the simulation duration, assuming a temperature of $T = 2\times10^7$ K and mean mass per particle $m = m_H\mu$ where m_H is the mass of hydrogen and $\mu = 0.6$ for a sound speed of $c_s = \sqrt{\gamma k_B T/m} \approx 0.70$ Mpc Gyr^{-1}, the approximate sound crossing time across the inner $R = 0.5$ Mpc, where the majority of the dynamics of the galaxy cluster evolves, is approximately 1.4 Gyr.

We used the ZEUS solver for hydrodynamics (Stone & Norman 1992) due to its robustness to evolve through discontinuities in the fluid around the AGN due to sharply peaked thermal injection. ZEUS is a relatively diffusive solver and requires an artificial viscosity, which may affect the accuracy of the hydrodynamics simulation (Stone & Norman 1992; Meece Jr 2016). Tabulated cooling was used to model radiative cooling following Schure et al. (2009), assuming a metallicity of 0.5 $Z_\odot$. The cooling table has a temperature floor of 10^4 K; any processes below this temperature will take place on a smaller scale than can be accurately explored with our spatial resolution.

Simulation results were analyzed using `yt` (Turk et al. 2011).

2.2. *AGN Feedback*

In the simplified AGN feedback model we used, feedback energy was deposited purely as thermal energy in a sphere centered on the cluster center, with the total amount of heating set equal to the total cooling in the cluster. Heating per unit volume was distributed following a power law in radius, as $\dot{e}(r) \propto r^{-\alpha}$. This basic power-law functional form has several numerical and practical issues. Most critically, these issues are a volumetric heating rate that diverges to infinity at the cluster center, a "long tail" of heating at the cluster outskirts where cooling is too slow to be relevant, and an unrealistic hard cutoff at the simulation boundaries. These latter two issues are compounded by observations that suggest AGN feedback is generally constrained to be within a few hundred kpc of the cluster center. To address these issues and to create a more tunable and effective heating kernel, we added two parameters: a minimum truncation radius r_s (effectively a smoothing length) and an exponential decay cutoff radius r_c. The feedback is also constrained to a fixed hard boundary radius of $R = 1.5$ Mpc. The full form of the volumetric feedback kernel is

$$\dot{e}(r,t) = \frac{\dot{E}(t)}{A}\begin{cases} \left(\frac{r_s}{r_c}\right)^{-\alpha}\exp\left(-\frac{r_s}{r_c}\right) & \text{erg s}^{-1}\text{ cm}^{-3}, \quad r \le r_s \\ \left(\frac{r}{r_c}\right)^{-\alpha}\exp\left(-\frac{r}{r_c}\right) & \text{erg s}^{-1}\text{ cm}^{-3}, \quad r_s < r \le R \\ 0 & \text{erg s}^{-1}\text{ cm}^{-3}, \quad R < r \end{cases}, \quad (7)$$

where $\dot{E}(t) = dE(t)/dt$ is the total energy feedback from the energy at time t, which we set to the total cooling within R. The scalar A is used to normalize the feedback, defined as

$$A = \int_0^\pi\int_0^{2\pi}\int_0^{r_s} dr d\phi d\theta \sin^2\theta \left(\frac{r_s}{r_c}\right)^{-\alpha}\exp\left(-\frac{r_s}{r_c}\right) \quad (8)$$

$$+ \int_0^\pi\int_0^{2\pi}\int_{r_s}^{R} dr d\phi d\theta \sin^2\theta \left(\frac{r}{r_c}\right)^{-\alpha}\exp\left(-\frac{r}{r_c}\right) \quad (9)$$

$$= \frac{4\pi}{3}\exp\left(-\frac{r_s}{r_c}\right) r_s^3 \left(\frac{r_s}{r_c}\right)^{-\alpha} \quad (10)$$

$$+ 4\pi r_c^3\left[-\Gamma\left(3-\alpha, \frac{R}{r_c}\right) - \Gamma\left(3-\alpha, \frac{r_{\rm min}}{r_c}\right)\right], \quad (11)$$

where $\Gamma(s,x) = \int_x^\infty t^{s-1}e^{-t}dt$ is the upper incomplete gamma function. Higher values of α correspond to more centralized feedback around the AGN. Without the inner smoothing length, a heating kernel with $\alpha \ge 3$ is not normalizable,

[1] This mass profile was used in Meece et al. (2017), but that paper did not correctly describe the mass profile because of a programming typo. Additionally, the gravitational acceleration used to generate the initial conditions from hydrostatic equilibrium erroneously uses a scale radius of 4Mpc instead of 4kpc. However, this does not substantially affect gravitational acceleration, densities, pressures, and other quantities outside of 1 kpc and does not affect our results.

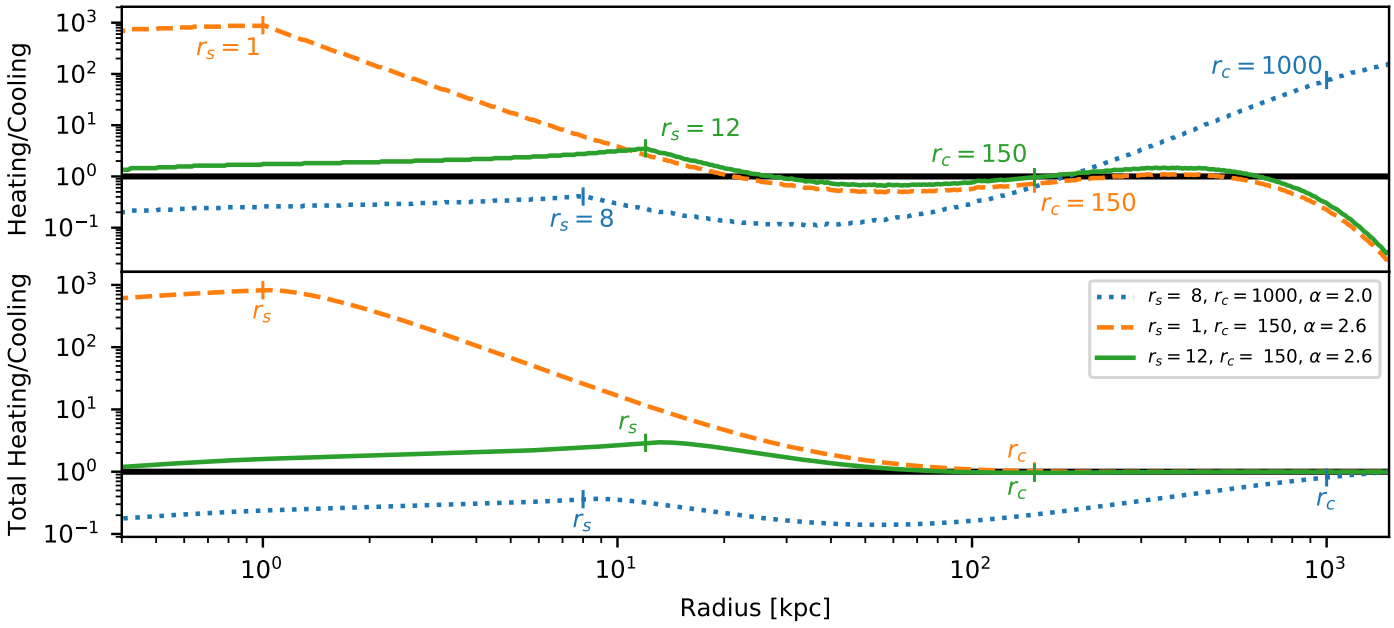

Figure 1. Top: Local ratio of heating to cooling as a function of radius (r) at the beginning of several representative simulations. The dotted blue line shows a simulation with low central heating and heating kernel parameters $\alpha = 2.0$, $r_s = 8$ kpc, and $r_c = 1000$ kpc. The dashed orange line shows a simulation with high central heating and heating kernel parameters $\alpha = 2.6$, $r_s = 1$ kpc, and $r_c = 150$ kpc. The solid green line shows a simulation with intermediate central heating and heating kernel parameters $\alpha = 2.6$, $r_s = 12$ kpc, and $r_c = 150$ kpc. **Bottom:** Cumulative ratio of heating to cooling within r for the same simulations. At large radii, all of the cumulative heating curves converge to the cumulative cooling rate because total heating is normalized to equal to total cooling rate at $R = 1.5$ Mpc.

because integration over a volume containing the origin diverges.

The total heating rate $\dot{E}(t)$ is set to the total cooling rate within the cluster. Since the total cooling rate can be difficult to compute on-the-fly due to the nature of the AMR hierarchy's timestep update, it is recomputed only every 10 Myr. Although the cooling rate increases exponentially leading up to a cooling catastrophe, the increase is slow enough so that the heating rate does not fall behind the true cooling rate by more than a few percent except immediately within a Myr before the catastrophe, at which point the simulation already shows that the parameters for AGN feedback are undesirable.

We tested 91 different kernels with a range of parameters: different radial exponents $\alpha \in [2.0, 3.2]$, smoothing lengths $r_s \in 1, 4, 8, 10, 12, 16, 20, 40$, and exponential cutoff radii $r_c \in 100, 150, 200$). We began our exploration of the parameter space by setting $r_s = 1$ and $r_c = 1500$ and sampled the range of α before trying different values of r_s and r_c with a smaller number of α values, seeking parameter choices that seemed closest to an optimal kernel. Figure 1 presents a representative sampling of heating kernels showing the initial ratio of heating to cooling as a function of radius, including both the local ratio at each radius and the cumulative ratio within each radius.

The AGN feedback implementation used in this work was modified from Meece Jr (2016); Meece et al. (2017) to match the AGN heating rate with the total cooling rate and allow feedback over a larger radius.

3. RESULTS

All the heating kernels we explored resulted either in cooling catastrophes within a few Gyr, central entropy levels greater than observations, or both. Simulations that eventually formed cold, condensed gas all went through cooling catastrophes. In those simulations, the minimum entropy drops over time, eventually leading to multiphase condensation. As cold clumps of gas form and runaway cooling begins, the requirement for total heating to match total cooling causes the heating rate to spike. The time required for cold gas to form is roughly correlated with the smallest radius at which cooling exceeds heating. If central cooling exceeds central heating, the cluster quickly forms cold gas and experiences a cooling catastrophe. Simulations with higher central heating tend to have high central entropy, similar to observations of NCC clusters. If the heating exceeds cooling out to radii of several tens of kpc, then the simulations persist for many Gyr without forming cold gas.

Figure 2 schematically shows the general behavior of the different heating kernels. The three heating kernel examples in Figure 1 have colors that match the corresponding schematics in Figure 2. Figure 3 shows mass density profiles of cooling rate, heating rate, and entropy at later moments in simulations employing the same three heating kernels as in Figure 1.

3.1. *Categorization of Simulations*

The results of our simulations can be grouped according to the morphology of the entropy profiles that develop within the central 100 kpc:

1. **Central Cooling.** The entropy profiles of simulated clusters with heating that is insufficient to balance radiative cooling at small radii develop central cooling flows with a positive entropy gradient at all radii. They undergo a central cooling catastrophe relatively quickly, in which runaway multiphase condensation at small radii brings the simulation to a halt.

2. **Central Convective Zone.** The entropy profiles of simulations with high central heating form an inner con-

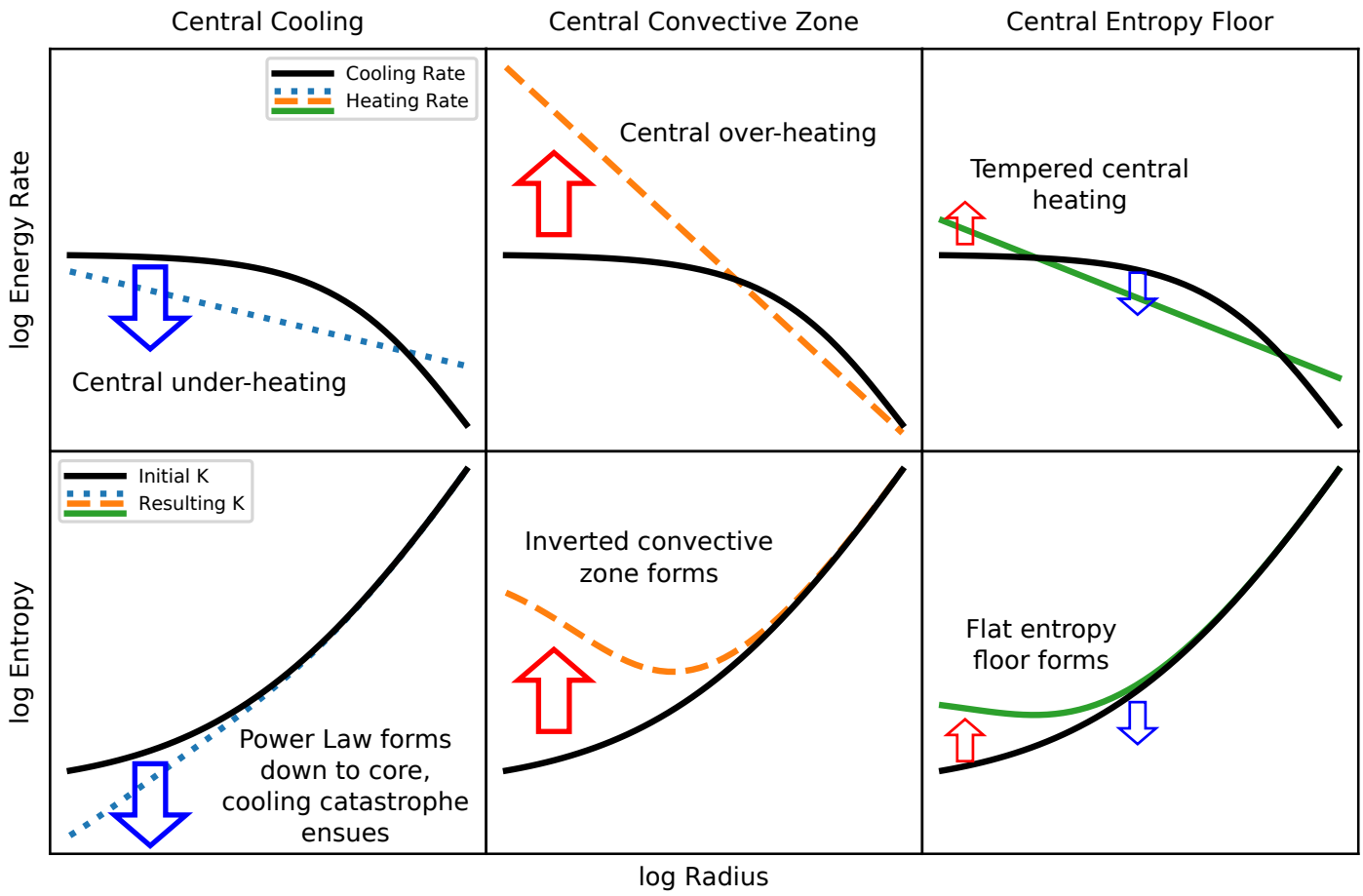

Figure 2. Schematic illustrations of how different AGN heating kernels affect the entropy profile of a simulated galaxy cluster. In each case, the total heating rate is set equal to the total cooling rate. **Top:** Radial profiles of radiative cooling and AGN heating per unit volume, with the initial median cooling rate in black and the AGN heating kernel in color. **Bottom:** Response of the median entropy profile to heat input. The initial median profile in black and the response is in color. The left column shows a heating kernel with central heating that falls below central cooling. The entropy profile in this case tends to follow a power law down to the origin and eventually leads to a central cooling catastrophe. The center column shows a heating kernel with excessive central heating, which elevates central entropy, inverts the entropy profile, and produces a central convective zone. The right column shows a heating kernel with intermediate central heating, which slightly raises the central entropy and produces a flat core.

vective zone with high central entropy and a negative central entropy gradient. Those simulations persist the longest before undergoing cooling catastrophes.

3. **Central Entropy Floor.** Simulations with intermediate central heating can maintain a nearly flat entropy gradient within the central $\sim$ 10 to 20 kpc.

For the purposes of our analysis, we define these categories based on the entropy within the inner 25 kpc. We categorize as Central Cooling those simulations whose average minimum entropy remains below 12 keV cm^2 (2/3 of the the initial minimum central entropy of 18 keV cm^2) . The Central Convective Zone simulations are defined to have maximum central entropy above 50 keV cm^2 (equal to the initial mean entropy of the inner 100 kpc). No simulation meets both of these criteria, so there is no overlap of these first two groups. The remaining simulations, which have minimum central entropies above 12 keV cm^2 and maximum central entropies below 50 keV cm^2, are categorized as Central Entropy Floor simulations.

The schematic diagrams in Figure 2 illustrate the general behavior of the different categories. Figure 3 shows representative snapshots of both cooling rate and entropy versus radius. Some of our simulations exhibit behavior from multiple categories at different times in their evolution. The following subsections describe each category in more detail.

3.1.1. *Central Cooling*

Simulations with low α, large r_c, or large r_s tend to have central cooling exceeding central heating, which quickly leads to a cooling catastrophe. The left column in Fig. 3 shows an example of such a simulation. Within the inner 10 kpc, the heating rate ranges from half the cooling rate to more than an order of magnitude less than the cooling rate. Because the central heating is insufficient to counteract a growing mass of strongly cooling gas at the cluster center, the simulation produces a cooling catastrophe within 2 Gyr. However, up to the moment at which a substantial quantity of cold gas forms, the entropy profile remains close to the initial state and similar to the cool-core clusters in the ACCEPT data set.

3.1.2. *Central Convective Zone*

Heating rates within the central $\sim$ 10 kpc of simulations with high α, small r_c, or small r_s tend to greatly exceed radiative cooling. The middle column in Fig. 3 shows an

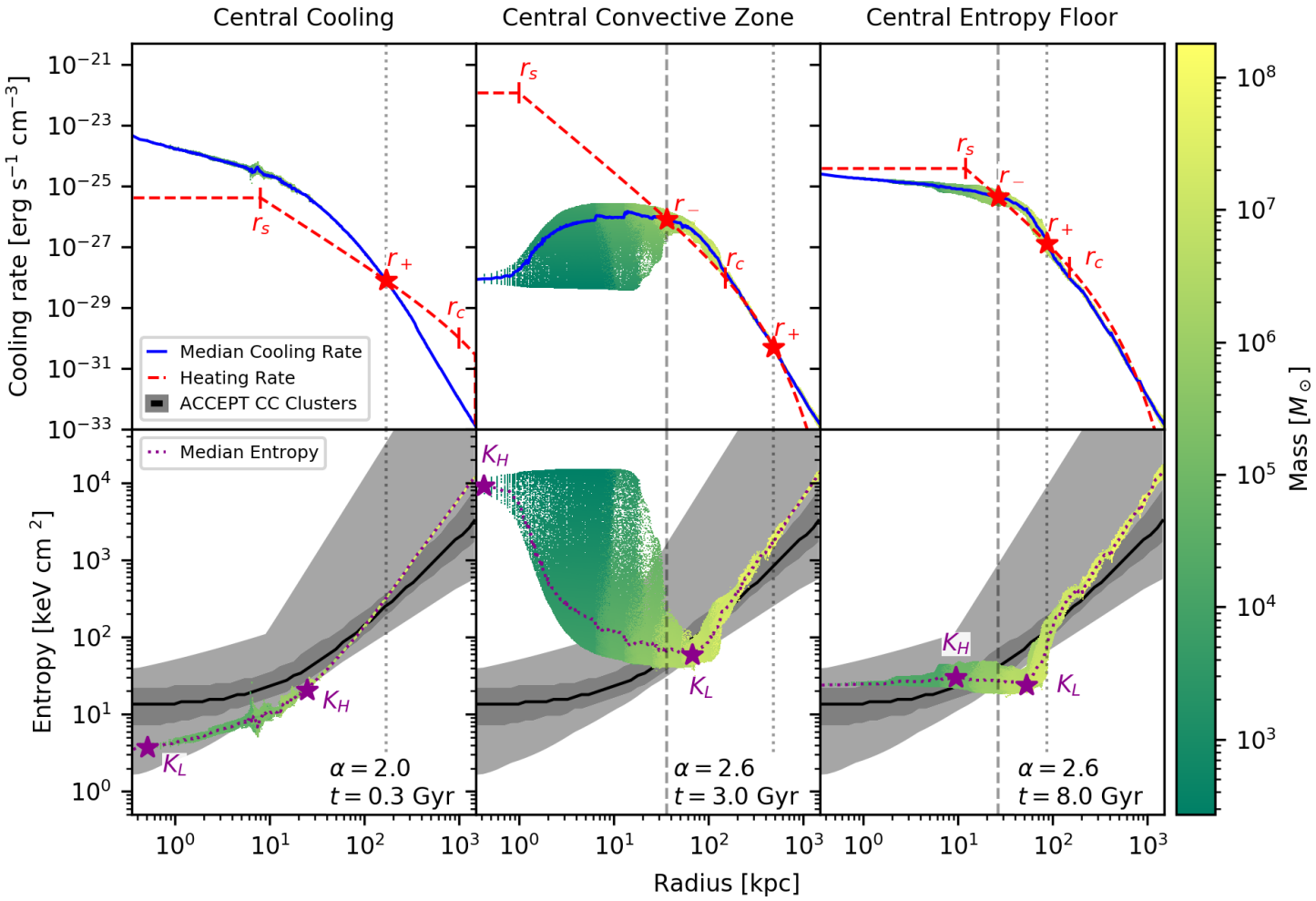

Figure 3. Mass density plots of cooling and heating rate (**top**) and entropy (**bottom**) versus radius of three simulations at different times that broadly represent the whole set of simulations, as differentiated by the behavior of the inner tens of kpc. The left column shows a simulation (with $\alpha = 2.0$, $r_s = 8$ kpc, and $r_c = 1000$ kpc at $t = 0.3$ Gyr) with low central heating leading to excess central cooling that quickly undergoes a cooling catastrophe. The middle column shows a simulation (with $\alpha = 2.6$, $r_s = 1$ kpc, and $r_c = 150$ kpc at $t = 3.0$ Gyr) with high central heating that maintains a convective zone in the inner 100 kpc with a high central entropy peak. The right column shows a simulation (with $\alpha = 2.6$, $r_s = 12$ kpc, and $r_c = 150$ kpc at $t = 8.0$ Gyr) with an intermediate amount of central heating and that holds a flat entropy floor slightly elevated from the initial conditions and observational data on the entropy of the inner tens of kpc. On the entropy plots, observational entropy data of clusters from the ACCEPT data set are displayed in grayscale showing the range, 68% confidence interval, and median of the dataset. The median entropy is also marked by a magenta line, and the minimum (K_L) and maximum (K_H) values of the entropy median within the inner 25 kpc are marked by stars. On the cooling rate plots, the heating rate is marked by a red line and the median cooling rate is marked by a blue line. The crossover radii r_- and r_+ as defined in the text are marked by stars in the simulations where they can be defined.The heating curve parameters r_s and r_c are also annotated with finely dashed and dashed gray lines.

example. Excess central heating leads to a central entropy peak and an inverted entropy profile that drives convection. Low-entropy gas at the minimum entropy point sinks toward the center, but is reheated there and eventually rises to larger radii. Such a convective configuration can persist for many Gyr without producing multiphase condensation, because the minimum entropy and minimum cooling time are both large.

A few of the simulations in this category do form multiphase gas. When that happens, condensation first appears at the minimum of the entropy profile and rapidly leads to a cooling catastrophe. Although these simulations have large central heating rates, the heating rate still falls below cooling at intermediate radii (near the entropy minimum), allowing large clumps of cold gas to form there. In all cases in which a convective central zone forms, the central entropy is excessive compared with observed CC clusters, in some cases being more typical for a NCC.

3.1.3. *Central Entropy Floor*

Simulations with intermediate central heating, corresponding to a narrow range of combinations of α, r_s, and r_c, are able to maintain quasi-stable flat entropy profiles out to radii exceeding 10 kpc. The right column in Fig. 3 shows an example. Central heating within the inner 10 kpc of these simulations is typically several times the central cooling rate, sufficient to offset runaway cooling but not great enough to produce a large entropy inversion. Only some of these simulations form cold gas, and typically do so at larger radii and later times than in the Central Cooling simulations. However, the central heating in these simulations is still great enough to elevate the central entropy above the values observed in CC clusters.

3.2. *Important radii: r_L, r_H, r_-, r_+, and r_{multi}*

To help with the analysis of the simulations, we identify several quantities that proved to be useful for interpreting their behavior. Those quantities are labeled in Figure 3.

The maximum and minimum entropy levels in the central regions turn out to be closely related to the time it takes for a cooling catastrophe to manifest. To quantify those extremes we first determine the median entropy at each radius, illustrated by the purple dotted lines in Figure 3. We then define K_L to be the minimum of the median entropy profile and r_L to be the radius at that point. Outside of r_L the median entropy profile is stable to convection, but inside of r_L it is convectively unstable. In simulations with low central heating, r_L is close to the center. We define K_H to be the maximum of the median entropy profile within $R = 25$ kpc and r_H to be the radius at that point. We use the 25 kpc cutoff to exclude cosmologically heated gas at large radii region from the analysis in order to focus on the effects of feedback heating. The initial entropy at 25 kpc is just below 30 keV cm^2, so a persistent K_H above 30 keV cm^2 indicates that heating has elevated the central entropy, making it too great for a CC cluster and possibly producing a central convective zone.

The entropy extrema K_L and K_H and the corresponding radii r_L and r_H evolve over time as feedback alters the median entropy profile. We denote the cooling times at those radii by $t_c(r_L)$ and $t_c(r_H)$. The value of $t_c(r_L)$ is closely linked to the time required for condensation to begin. Figures 5, 6, and 7 show how the heating kernel parameters affect K_H and K_L, along with the associated radii and cooling times.

The radii at which heating equals cooling are special and come in two types. For one type, the net heating rate goes from positive to negative as r increases. We define r_- to be the smallest such radius. Excess heating within that radius tends to raise the median entropy while excess cooling at large radii causes the median entropy to decline. The result is flattening and sometimes inversion of the median entropy profile, which drives convection and ultimately makes the system prone to condensation near r_-. However, if cooling dominates heating in the central regions, then r_- is undefined. Some relationships between r_- and the simulation outcomes are shown in Figure 5.

At the other type of heating-cooling equality radius, the net heating rate goes from negative to positive as r increases. We define r_+ to be the largest such radius. Outside of r_+, net heating raises the median entropy and suppresses condensation. Within r_+, net cooling lowers the median entropy. Together, these effects produce a positive entropy gradient in the vicinity of r_+.

While the median cooling rate may exceed the heating rate at very large radii (on the order of hundreds of kpc), cooling times at those radii are so long that cold gas does not form on an astrophysically significant time scale. During a given simulation, the radii r_- and r_+ do not stay fixed, but rather shift as heating and cooling change the median cooling rate. We denote the cooling time at those radii as $t_c(r_-)$ and $t_c(r_+)$.

The heating kernel parameters also affect when cold gas forms in the simulations and at what radius the cold gas first appears. We define $t_{\rm multi}$ to be the time from the beginning of the simulation to the moment when multiphase condensation produces cold gas. We define $r_{\rm multi}$ to be the radius at which cold gas first appears. As shown in Figure 5, the radius $r_{\rm multi}$ is weakly connected to r_H and $t_{\rm multi}$ is tightly connected to $t_c(r_-)$. Simulations that never form cold gas are assigned $t_{\rm multi} = 16$ Gyr in that figure and do not appear on plots showing $r_{\rm multi}$ because it is undefined.

3.3. *Condensation of Cold Gas*

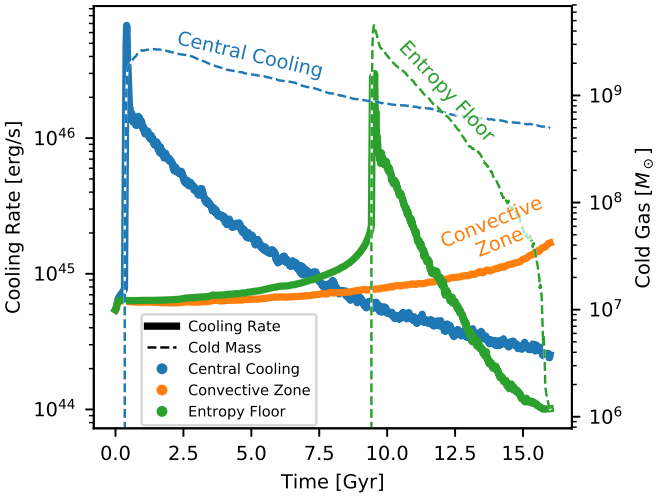

Figure 4. Time dependence of total cooling rate (solid lines) and total mass of condensed gas under 3×10^4 K (dashed lines) for the three simulations shown in Figure 3. The blue points show a simulation with low central heating and excess central cooling ($\alpha = 2.0$, $r_s = 8$ kpc, $r_c = 1000$ kpc) that experiences an early cooling catastrophe. Orange points show a simulation with high central heating ($\alpha = 2.6$, $r_s = 1$ kpc, $r_c = 150$ kpc) that forms a quasi-stable central convective zone. Green points show a simulation with intermediate central heating ($\alpha = 2.6$, $r_s = 12$ kpc, $r_c = 150$ kpc) that maintains a flat entropy core for almost 10 Gyr before undergoing a late cooling catastrophe. In simulations that form a multiphase gas through a cooling catastrophe, the formation of cold gas is preceded by a rise and then a sharp peak in the total cooling rate.

Multiphase condensation forms cold gas in many of the simulations, in each case leading to a cooling catastrophe. Cold gas starts forming near r_L, then falls toward the center, displacing buoyantly rising warmer gas. The location of r_L depends on the heating kernel parameters and is related to r_-.

However, when gas at r_L cools enough to transition into the cold phase, it sharply raises the total cooling rate of the cluster. That event immediately boosts the heating rate by the same factor, because our AGN feedback prescription forces the total heating rate to equal the total cooling rate. This heat is distributed across the cluster and is not concentrated on the cooling gas, and thus the AGN feedback does not halt the cooling catastrophe.

In many cases, rapid heating of lower-density gas during the cooling catastrophe accelerates it to such high speeds and creates such large discontinuities in the fluid that the simulation becomes infeasible to continue due to the Courant condition. At that point the heating input greatly exceeds the AGN activity observed in real CC clusters, meaning that the chosen heating kernel has become physically unrealistic. In simulations that managed to evolve through this catastrophic event, the heat input leads to drastically elevated entropy in the ambient gas, which slowly reheats the embedded cold gas and prevents more cold gas from forming. After the cold gas is reheated, the core entropy is left much higher than before the catastrophe. Figure 4 illustrates the timeline of a catastrophe resulting from an increasing cooling rate that leads the formation of cold gas.

Our simulation set generally demonstrates that the radii $r_{\rm multi}$ and r_L are both related to r_-. Figure 5 shows the relationships among the time-averaged values of those three radii. Larger r_- corresponded to a larger r_L. Larger r_- and r_L also correspond to cold gas first forming at a larger radii (larger $r_{\rm multi}$). The relationship between r_- and the formation of cold

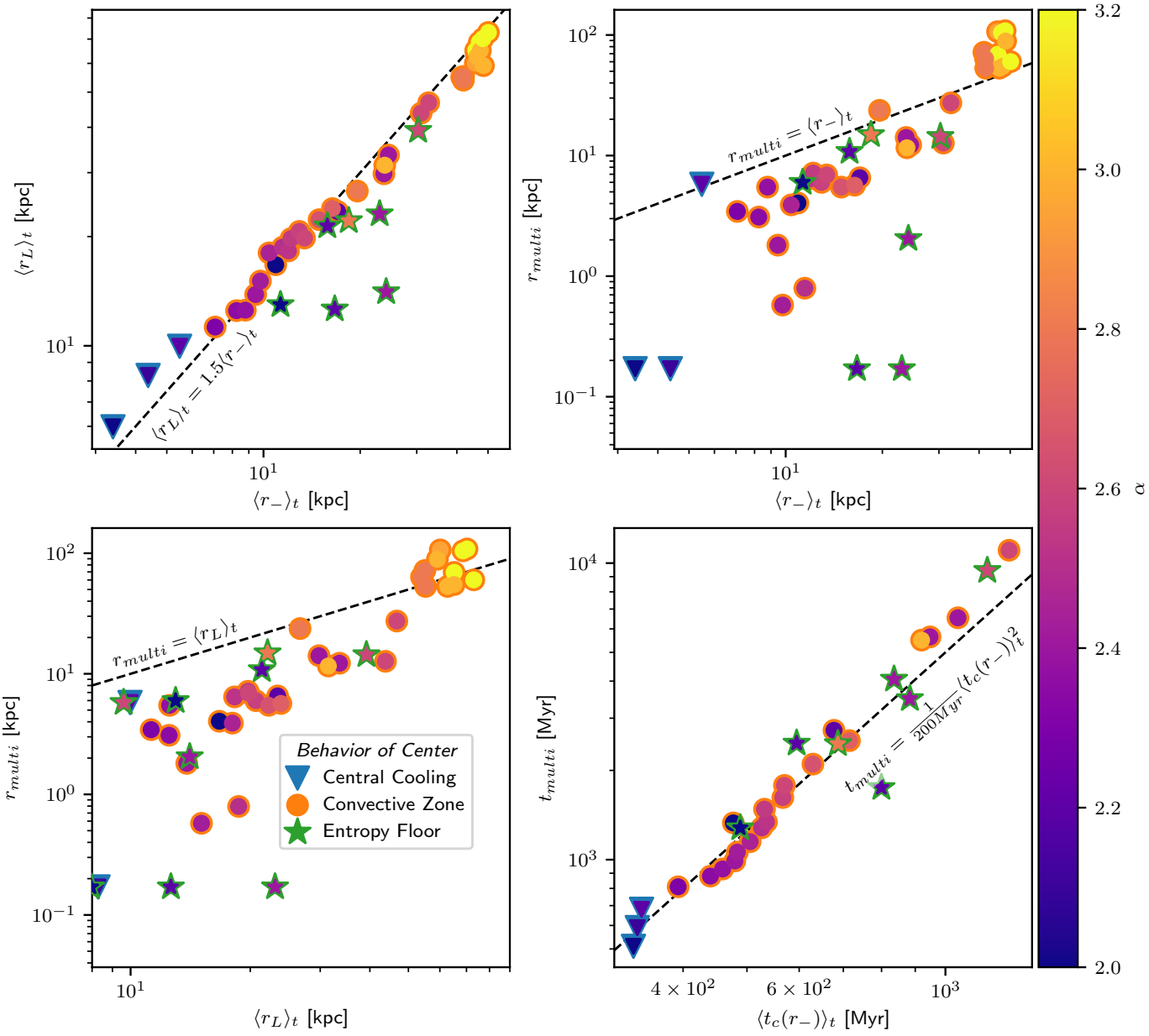

Figure 5. Plots of relationships between r_-, the radius at which the gas switches from net heating to net cooling, and other features of the simulations. **Top left:** Time averaged radius of the minimum of the median entropy profile (r_L) versus the time average of r_- up to the formation of a multiphase gas. (Includes only simulations in which r_- can be defined for at least 50 Myr.) **Top right:** Radius at which multiphase gas first forms versus the time averaged r_-. (Includes only simulations in which r_- can be defined for more than one time step.) **Bottom left:** Radius at which multiphase gas first forms versus the time averaged value of r_L for all simulations. **Bottom right:** The time required for a simulation to form multiphase gas versus the time averaged value of the cooling time at r_-. (Includes only simulations that form multiphase gas and in which r_- can be defined for at least 50 Myr.) Shapes in each panel denote the general behavior of the central region of the simulation. Blue highlighted triangles denote Central Cooling simulations, orange highlighted circles denote Central Convective Zone simulations. Green highlighted stars denote Entropy Floor simulations. Colors show the heating kernel parameter α, with greater α generally corresponding to heating that is more centrally concentrated.

gas is most apparent in the plot of $t_c(r_-)$ versus $t_{\rm multi}$. When r_- is larger, the cooling time r_- is longer, which leads to cold gas forming later in the simulation. The timescale on which cold gas forms is closely tied to the cooling time of this gas. Interestingly, the relationship is non-linear, following

$$t_{\rm multi} = \frac{1}{200\ {\rm Myr}} \langle t_c(r_{\rm multi}) \rangle^2. \quad (12)$$

This result is consistent with previous work by Meece et al. (2015) exploring the condensation of gas in the central ICM of galaxy clusters. Meece et al. (2015) found in ICM simulations with varying initial $t_{\rm cool}/t_{\rm fall}$ that gas with longer cooling times takes more cooling times to condense into a multiphase gas, suggesting a non-linear relationship between cooling time and the formation of cold gas.

3.4. *Central Heating*

The heating kernel parameters also affects the central entropy of the cluster, in some cases resulting in unreasonably high levels for a CC cluster and in other cases allowing cold gas to quickly condense and collect in the cluster center. The central entropy and general behavior of the core is directly

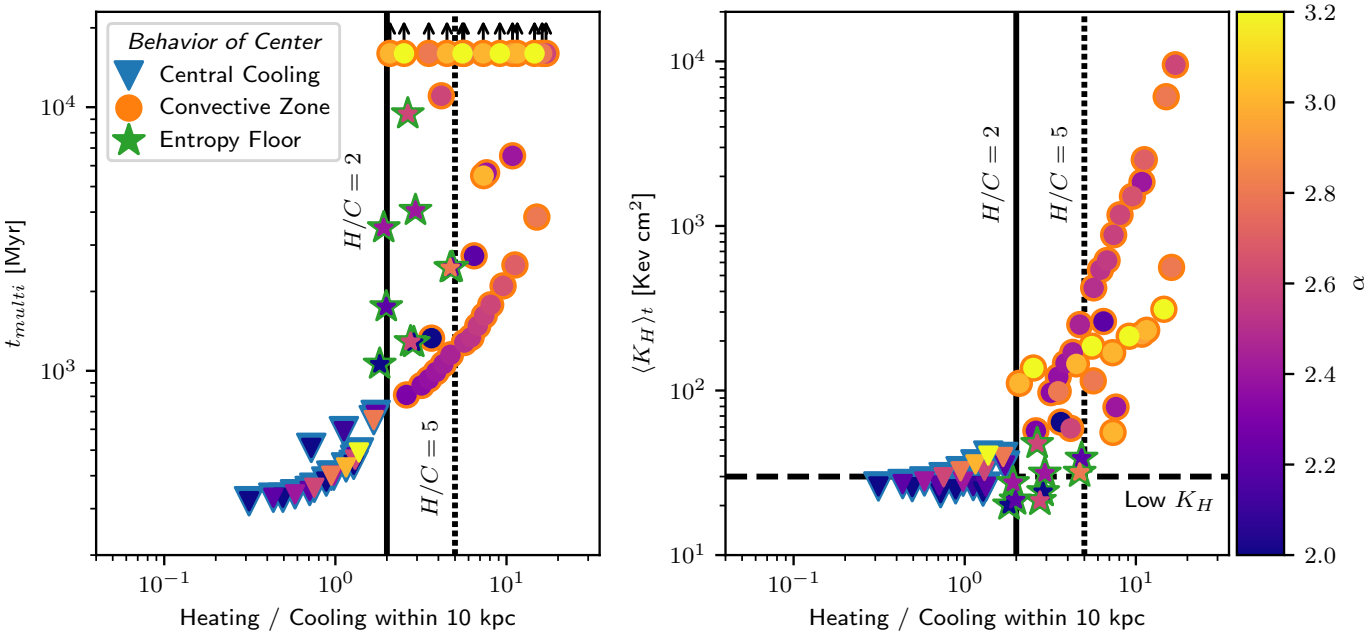

Figure 6. Left: Time required to form multiphase gas in a simulation versus the ratio of heating to cooling within the inner 10 kpc at the first time step. **Right:** Maximum of the median entropy within the inner 25 kpc, versus the ratio of heating to cooling within the inner 10 kpc at the first time step. In both panels, a solid line marks a heating to cooling ratio of 2, and a dashed line marks a heating to cooling ratio of 5. A ratio of at least 2 is required to avoid multiphase condensation within 1 Gyr. In the right panel, a dashed line marks the maximum central entropy that is observationally expected for a CC cluster.

related to the amount of heating compared to cooling in the cluster center. A certain amount of heating in the center is necessary to offset the central cooling but an excess of heating in the cluster center causes central entropies higher than observed in CC clusters.

To explore this behavior, we track the ratio of the total heating within the inner 10 kpc of the cluster to the total cooling within the same volume.[2] Figure 6 shows $t_{\rm multi}$ and the time average of K_H versus the initial central heating to cooling ratio. A ratio of heating-to-cooling of approximately two is needed to maintain quasi-stability for any significant amount of time, while a ratio greater than five always leads to high central entropies. Inside this range of ratios of heating to cooling, different heating kernels produce all three categories of central entropy behaviors.

When the integrated heating in the inner region is less than twice the cooling in the same region, a cooling catastrophe happens within 1 Gyr. For simulations with less heating than cooling in the central region, cooling quickly causes the central entropy profile to approximate a power law down to the cluster center. Cooling gas then flows down the entropy gradient, collecting in the center, and forming multiphase gas. In simulations with average heating one to two times the average cooling rate in the center, density inhomogeneities in the gas allow cooling to exceed heating in some locations. As the cooling of that gas increases, the total heating rate rises but is insufficient to counter the localized increase in cooling, thus leading a runaway cooling catastrophe. Additionally, as central entropy falls and density increases in the lead up to the catastrophe, central pressure increases and compresses clumps of cooling gas. This further accelerates their cooling during the runaway catastrophe. With simulations having heating-to-cooling ratios above two in the center region, the central cooling is more successfully countered so that the formation of multiphase gas happens on a longer timescale connected to $t_c(r_L)$ and $t_c(r_-)$, as discussed in Section 3.3. The left plot in Figure 6 also shows this distinction in behavior.

When central heating rates are more than two times greater than the cooling rate, excess heating leads to central entropies that are higher than what is observed for CC clusters. The right plot in Figure 6 shows the relationship between the ratio of central heating to cooling and the maximum entropy in the central region averaged over time. Some simulations with two to five times heating to cooling in the center stay under the typical 30 keV cm^2 specific entropy for CC clusters, but all of the simulations with heating-to-cooling ratios of greater than five produce unrealistically high entropies. With values of K_H above the 30 keV cm^2 specific entropy where the isentropic entropy profile changes into power law, these simulations form an inverse convective zone where hot gas collects in the cluster center and cold gas collects at r_L at intermediate radii.

4. DISCUSSION

4.1. *No Adequate Heating Kernel*

None of the 91 heating kernels we simulated meet all three of the adequacy criteria specified in Section 1. The failure modes we observe in the simulations can be discussed in terms of the same behavioral categories listed in Section 3.1 for the central entropy profile:

1. **Central Cooling.** Heating kernels with low central heating fail to meet our first criterion by producing a cooling catastrophe within ~ 1 Gyr that radically changed the structure of the ambient medium.

2. **Central Convective Zone.** Heating kernels with high central heating produces central convective zones that fail to meet our second criterion by producing central

[2] The inner 10 kpc volume was chosen to coincide with the region within which the initial entropy profile is nearly flat. We also tested this analysis using the inner 20 kpc volume and found similar results.

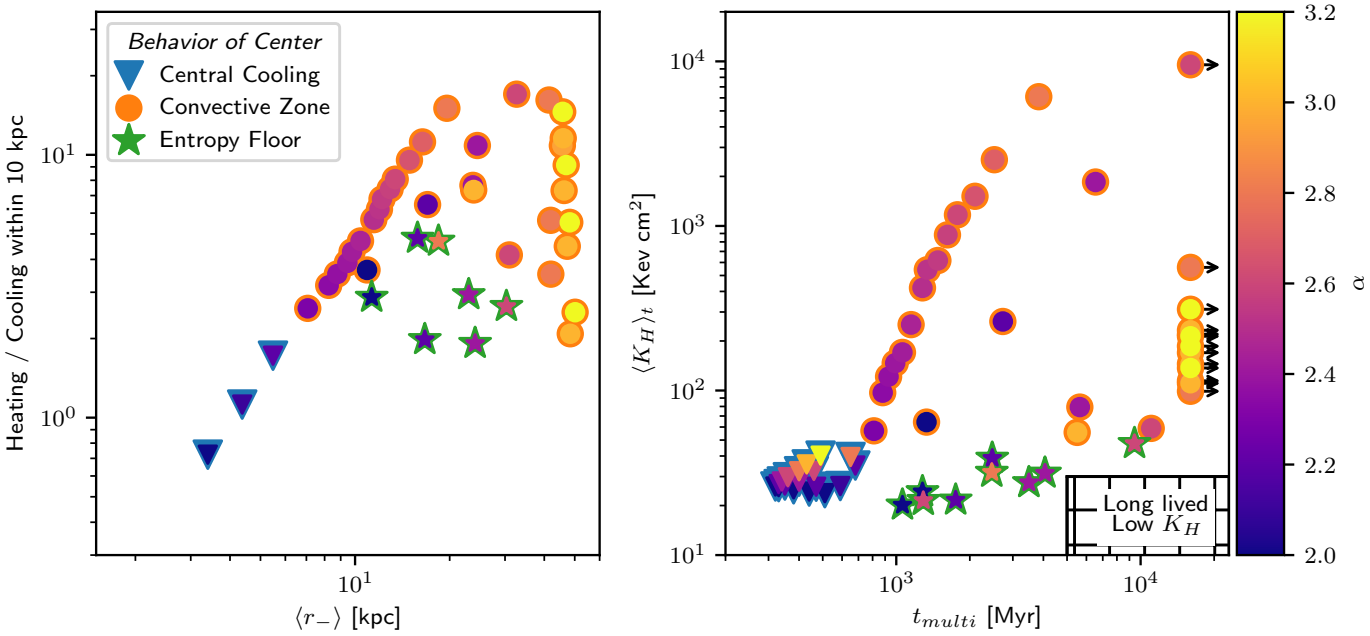

Figure 7. Left: Relationships between the initial ratio of heating to cooling averaged over the inner 10 kpc and the time-averaged radius $\langle r_- \rangle$ beyond which cooling begins to dominate over heating. Only those simulations in which r_- can be defined for at least 50 Myr are included. The box in the lower right shows hypothetical simulations with an average r_- over 30 kpc and an inner heating to cooling ratio under five. **Right:** Relationships between the time average of K_H (the maximum level of the median entropy profile within the inner 25 kpc) and the time $t_{\rm multi}$ until multiphase gas forms in the simulation. The plot includes all simulations, assigning $t_{\rm multi}$ = 16 Gyr to simulations that do not form cold gas by that time. An empty box in the lower right corner indicates where points representing heating kernels satisfying adequacy criteria would fall, by persisting for more than 5 Gyr before forming multiphase gas while maintaining a maximum entropy level < 30 keV cm^{-2} within 25 kpc. However, no heating kernel we tested satisfies those those criteria.

entropy levels greatly exceeding those observed among typical CC clusters. Some of the simulations in this group also fail our longevity criterion because the heating kernel is unable to prevent an early cooling catastrophe due to insufficient heating at intermediate radii.

3. **Central Entropy Floor.** The heating kernels closest to being adequate, according to our criteria, were those with intermediate central heating that exceeds central cooling, but not by a large factor. Those simulations maintain a quasi-stable entropy floor and prevents cooling catastrophe for billions of years. However, the central entropy profiles of those simulations, while lower than those in the previous category, were still elevated compared to observed CC clusters and thus do not meet our second criterion. Lowering the central heating rates in an attempt to bring their entropy profiles more in line with observation also causes cold gas to form much more quickly. The simulation that provides results closest to a realistic cluster maintains a flat entropy core of 30 keV cm^2 and lasts for just under 4 Gyr, which may be sufficiently long to maintain a CC cluster between external heating events.

No heating kernel we tested is able to maintain a low entropy floor close to observations of CC clusters for longer than 4 Gyr.

Figure 7 summarizes the failure modes of the heating kernels probed in this study. The right panel shows K_H versus $t_{\rm multi}$, a measure of the longevity of the simulation before a cooling catastrophe strongly altered it. Some simulations prevent a multiphase cooling catastrophe for many Gyr while others maintain low central entropy, but no heating kernel accomplished both aims. The left panel shows the ratio of central heating to cooling versus r_-, the two parameters that most strongly influenced the central entropy and longevity, respectively.

4.2. *Robustness of Feedback Algorithm*

The ultimate obstacle to finding an adequate thermal heating kernel is the difficulty of preventing gas in the cluster center from overcooling while still maintaining a reasonably low entropy profile. In order to prevent a cooling catastrophe, central heating must be sufficient to raise the median entropy profile enough to keep the lowest-entropy gas from undergoing runaway cooling. Our simulations show that an integrated central heating rate within the inner 10 kpc that is approximately two times the cooling rate in that same region is necessary. Otherwise, too large a proportion of the gas within the central region ends up with cooling exceeding heating, causing a rapid increase in the total radiative cooling rate.

The consequences of that rapid rise in cooling are dramatic, because the total heating rate is set equal to the radiative cooling rate and rises just as rapidly. However, that heat input is distributed more evenly across a large volume and cannot counteract radiative cooling of localized dense gas clumps. As a result, the ambient pressure sharply rises, compressing the dense clumps of low-entropy gas, causing both radiative cooling and the matching heating rate to increase. That coupling therefore causes the cooling/heating rate to spike to unphysically high levels during a cooling catastrophe (see Figure 4). Central internal energies and velocities then rapidly rise and create discontinuities in the fluid. Due to the Courant condition, the time steps sometimes became too small to continue evolving the simulations. In other cases, those discontinuities lead to negative densities and internal energies in the hydro solver, ultimately ending the simulation.

In reality, CC clusters can form cold gas (as is evident from

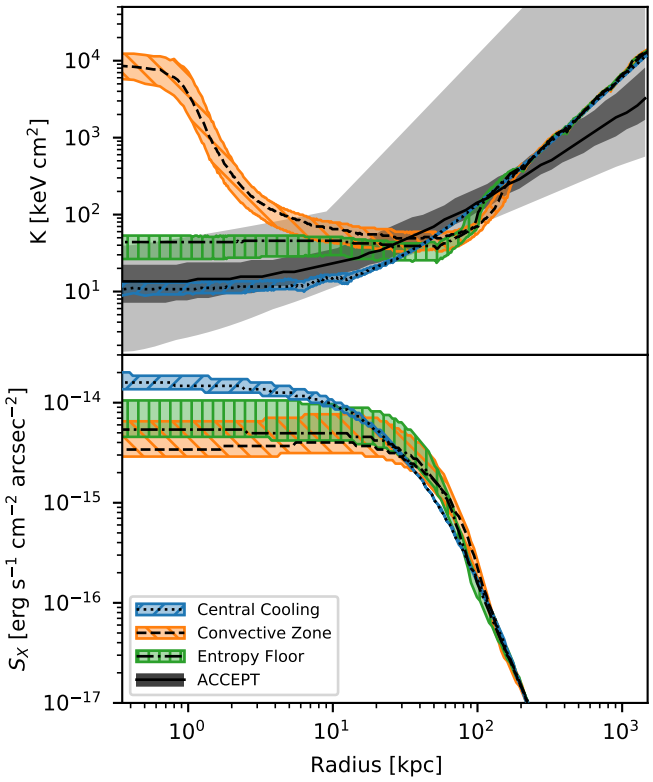

Figure 8. **Top:** Time-averaged median entropy profiles of the simulated clusters in Figure 3. The dotted line shows the simulation with low central heating ($\alpha = 2.0$, $r_s = 8$ kpc, $r_c = 1000$ kpc), and the blue shaded region around it shows the 1σ dispersion of its median profile over time. The dashed line shows the simulation with high central heating ($\alpha = 2.6$, $r_s = 1$ kpc, $r_c = 150$ kpc), and the orange shaded region around it shows its 1σ dispersion. The dot-dashed line shows the simulation with intermediate central heating ($\alpha = 2.6$, $r_s = 12$ kpc, $r_c = 150$ kpc), and the green shaded region around it shows its 1σ dispersion. In each case, entropy is weighted by the x-ray luminosity in the 0.5–2.0 keV band, to mimic data obtainable with *Chandra*. The median, 1σ interval, and full extent of the entropy profiles of CC clusters from ACCEPT are shown in grayscale. **Bottom:** X-ray surface brightness in the 0.5–2.0 keV band for the same simulated clusters, with shaded regions showing the 1σ dispersion and black lines showing the median.

observed star formation rates from ranging from 1 to 100 $M_\odot$ per year), and so a physically accurate model should accommodate the formation of moderate amounts of cold gas. However, a heating kernel that immediately responds by injecting compensating thermal energy with a fixed spatial distribution appears to be unable to accommodate multiphase condensation with causing excessive heating.

4.3. *Comparison to Observations*

Figure 8 shows the time-averaged median entropy profile and projected X-ray surface brightness profile, along with the 1σ dispersion in the median profiles. It also shows the median entropy profile of observed CC clusters in the ACCEPT dataset (Cavagnolo et al. 2009), along with the 1σ dispersion and the full range. The dispersion in the simulated profiles is computed in radial bins over the lifetime of each simulation up until the formation of cold gas or the end of the simulation. The dispersion in the ACCEPT data is generated from a table of power-law fits to the entropy profiles. Only CC clusters from ACCEPT with $K_0 < 30$ keV cm^2 are used.

No quasi-stable simulation maintains a central entropy close to the majority of the CC clusters in the ACCEPT dataset. Heating kernels that keep low entropies within the range of the ACCEPT CC clusters are not steady for more than 1 Gyr, and all experience central cooling catastrophes. Heating kernels that form central convective regions have higher central entropies than the ACCEPT CC clusters. Simulations that form a central entropy floor have lower entropies than the central convective zone simulations and are steady for longer periods than the low central heating kernels, but still have higher central entropies than the majority of observed CC clusters in the ACCEPT dataset.

The differences among the X-ray surface brightness profiles are more subdued, with more centralized feedback corresponding to a lower central surface brightness. The median central surface brightness of the simulation shown here with a central catastrophe is within an order of magnitude of the simulations that form a convective zone.

4.4. *Comparison to Other Simulations*

Thermal regulation of galaxy clusters by AGN jets has been studied previously through numerical simulation using many different models of AGN feedback. These approaches include injection of buoyant bubbles (Brüggen 2003b; Hillel & Soker 2016), magnetic fields (Li et al. 2006; Nakamura et al. 2006, 2007; Huarte-Espinosa et al. 2012), kinetic jets (Wu et al. 2015; Martizzi et al. 2016; Hahn et al. 2017; Meece et al. 2017), stochastic momentum feedback (Weinberger et al. 2017; Nelson et al. 2019), cosmic rays (Jubelgas et al. 2008; Butsky & Quinn 2018), and turbulent heating (Gaspari et al. 2012a; Zhuravleva et al. 2014; Banerjee & Sharma 2014), either explicitly or implicitly driven by the central SMBH. Some simulations have also used purely thermal feedback models like the model used in this work, to which we can compare.

Meece et al. (2017), the predecessor to this work, tested a AGN feedback model consisting of a precessing bipolar jet that injected kinetic and thermal energy. They tested different fractions of AGN feedback going into thermal heating versus the kinetic jet. For triggering the feedback they tested three different models: a cold gas triggering model from Li & Bryan (2014), a boosted Bondi-like triggering, and a Booth and Schaye accretion model (Booth & Schaye 2009). Like this work, Meece et al. (2017) found that AGN models with purely thermal feedback led to an overabundance of cold gas in the simulation core. However, their thermal feedback was limited to a small region around the AGN, less than 1 kpc in diameter. It was speculated that the overcooling occurred due to a lack of heating reaching outside of the cluster center. In their simulations, hot bubbles inflated via AGN heating at the cluster center buoyantly rose a short distance out of the center to $10-30$kpc to create a flatter entropy profile that was more unstable to multiphase condensation. The injected energy failed to escape to further radii outside the core. The work presented in this paper rectifies the small heating region shortcoming and is able to produce thermally steady clusters with purely thermal heating, but with elevated core entropy beyond what is reasonable for a CC cluster. However, by equating the heating to cooling globally our heating prescription is no longer robust to the formation of cold gas.

The RHAPSODY-G simulations of galaxy clusters explored cosmological zoom-in simulations with star formation and feedback (SFF) and supermassive black hole (SMBH) formation and feedback, using the RAMSES Eulerian AMR code (Wu et al. 2015; Teyssier 2002). In their AGN feedback prescription, mass accreted onto the SMBH following a density-boosted Bondi-Hoyle accretion rate (Booth & Schaye 2009).

Thermal energy was deposited into a small radius around the SMBH (Martizzi et al. 2016). Compared to CC cluster entropy profiles from the ACCEPT catalogue, CC clusters in the RHAPSODY-G had lower central entropies, showing overcooling in the inner tens of kpc (Hahn et al. 2017).

Tremmel et al. (2017) presented the ROMULUS galaxy simulations using the CHANGA smoothed particle hydrodynamics code and includes SMBH feedback and SFF models tuned to observations. Their SMBH feedback model had two free parameters: (1) the efficiency of the accretion rate onto the SMBH and (2) the gas coupling efficiency ϵ_c. These parameters were calibrated to produce galaxies with observed values of the stellar-mass to halo ratio, HI gas fraction as a function of stellar mass, galaxy specific angular momentum versus stellar mass, and the SMBH to stellar mass relation. Their simulations used a thermal-only feedback model that deposited feedback energy into the 32 gas particles nearest to the SMBH. Mass accretion was governed by a modified Bondi accretion rate. Gas cooling was suppressed when heated by the SMBH for a time step equal to the time step of the SMBH. This allowed energy to escape away from the SMBH, although it may not be physically realistic. This feedback model produced galaxies with regulated SFF compared to observation.

In the follow-up paper Tremmel et al. (2019) on the cosmological ROMULUSC simulations, the same SFF and SMBH feedback models were used in a zoom-in simulation of a single halo. In an isolated halo, purely thermal feedback from the SMBH led to a conic structure with a highly collimated jet-like outflow. The outflows evolved over time, changing in shape and direction with the angular momentum of the gas near the SMBH. Energy was carried out to large radii through the outflows, which suppressed cooling at large radii. Star formation rates were regulated and matched observed rates in clusters. Additionally, the entropy profile of the clusters was within the range of observed profiles in CC clusters. Although the outflows were not explicitly included in their feedback prescription, the presence of these outflows might have been key for the thermal regulation of their simulated CC clusters.

4.5. *Implications*

Since the heating kernels explored here failed to produce quasi-stable CC clusters with realistic entropy profiles, extrapolations to real CC clusters may not be accurate. However, a few lessons can be drawn from these simulations:

- In the context of purely thermal AGN feedback, feedback that is highly centrally concentrated and tied directly to the radiative cooling rate produces unphysically high entropy cores for CC clusters that exceed observations and in some cases are physically unreasonable.

- When the heating rate is directly tied to the total cooling rate in the cluster, the rapid cooling of gas into cold clumps causes the heating rate to reach unphysically high levels. In comparison, in simulations using Bondi accretion or cold gas accretion such as in Meece et al. (2017) the AGN feedback increases with the formation of cold gas, but the efficiency of energy feedback can be tuned to match physically reasonable values.

- The heating kernels considered here, in which heating per unit volume had a fixed radial distribution, were unable to maintain thermal stability of the cluster. In cases where a cold clump of gas formed, the purely thermal AGN feedback was insufficient to disrupt the clump without injecting unphysically high amounts of energy. The thermal heating in these simulations was unable to reproduce the effects caused by kinetic outflows from AGN jets such as in Meece et al. (2017).

A workable heating kernel for purely thermal feedback may exist but would need to have with different parameters than are explored here.

4.6. *Other Models Investigated*

In search of a workable kernel, we investigated several extensions to the simple spherically symmetrical feedback kernels described in Section 2. First, we applied a polar angle dependence of $\cos^2\theta$ to mimic the conical distribution of heat from a kinetic jet. Total heating remained linked to total cooling. However, decreased heating near the equatorial plane leads to cold gas forming several tens of Myr sooner than for the corresponding spherical kernel and did not change the general behavior of the cooling catastrophe. Next, we tried a model in which cold gas was removed from the center of the simulation as it formed, to decrease the central density, potentially avoid fluid discontinuities in the fluid solver, and allow robust simulations with the formation of cold gas. However, explosive heat input triggered by the formation of cold gas still causes the hydrodynamics solver to fail. We also tested fixing the total heating to the total cooling of only the warm gas, testing separately temperature thresholds of $10^{6.5}$ K and 10^7 K, to exclude the rapid cooling of cold gas and avoid explosive AGN feedback. However, this filtering of cold gas in the calculation of the heating rate leads to more cold gas forming and the leftover warm gas having an elevated central entropy. In some cases the heat input is still great enough to halt the simulation because of the Courant condition. Last, we tried smoothing out the rise in AGN heating by setting the total feedback to the average of the cooling rate over the last 50 Myr, in essence implementing a time kernel as well as a spatial kernel. However, this approach also leads to high rates of formation of cold gas due to the delayed heating response, as well as an eventual spike in AGN heating since the cooling catastrophe ultimately is not counteracted.

4.7. *Future Models*

There remain conceivable modifications to this heating kernel approach that we did not investigate, but which could produce more physically realistic CC clusters. For example, total heating could be capped at a physically reasonable value to avoid the overheating that coincides with the formation of cold gas. Additionally, we could investigate a radially piecewise conic feedback kernel in which AGN heating is spherically symmetric at small radii and conical at large radii. Another alternative would be a kernel with a spatial distribution that depends on the total heat input, adjusting to spikes in heating/cooling by distributing increased heating over a larger volume, as would happen with an increase in total jet power.

5. SUMMARY

We have presented simulation results for simplified models of AGN feedback using purely thermal feedback with a spatial dependence following a radial power law $\dot{e} \propto r^{-\alpha}$ having a smoothing length r_s at small radii, an exponential cutoff radius r_c at large radii, and a total heating rate set equal to the

total cooling rate measured within the cluster. All heating kernels tested with this model fail to maintain thermal stability while also having observationally reasonable entropy profiles (see Figures 3 and 7.) The purely thermal feedback was insufficient to suppress the formation of large clumps of cold gas even though the increased cooling rate raises the heating rate to very high levels.

We also compared entropy profiles from these results to observational data from the ACCEPT dataset. Some simulations exhibit small to large central peaks in entropy that differ significantly from the power-law entropy profiles seen in the ACCEPT sample. The entropy peaks are pronounced for higher values of α due to the more centralized feedback. Simplified AGN models with centralized thermal heating do not produce realistic entropy profiles.

A few lessons can be drawn from this work. Highly centralized feedback without kinetic outflows apparently produces unreasonable high entropy profiles compared to observations. That happens because an AGN heating rate that is directly tied to the radiative cooling rate leads to a sharp jump in feedback as cold gas forms. This approach differs from previous simulations approximating feedback rates using Bondi and cold gas accretion models, which can temper the feedback response. No configuration of purely thermal feedback explored here achieved thermal stability nor prevented a run away collapse into a cold clump, in contrast to previous simulations that included kinetic jets. A heating kernel for purely thermal AGN feedback that produces realistic CC clusters may still exist but would need to significantly differ from the kernels we tested.

6. ACKNOWLEDGMENTS

We thank Philipp Grete and Deovrat Prasad for useful discussions. We also thank Megan Donahue, Dana Koeppe, and Rachel Frisbie for assistance with the ACCEPT database.

This project has been supported by NASA through Astrophysics Theory Program grant #NNX15AP39G and Hubble Theory Grant HST-AR-13261.01-A, and by the NSF through grant AST-1514700. The simulations were run on the NASA Pleiades supercomputer through allocation SMD-16-7720 and at the Michigan State University High Performance Computing Center (operated by the Institute for Cyber-Enabled Research). `Enzo` and `yt` are developed by a large number of independent researchers from numerous institutions around the world. Their commitment to open science has helped make this work possible.

REFERENCES

Banerjee, N., & Sharma, P. 2014, Monthly Notices of the Royal Astronomical Society, 443, 687
Binney, J., & Tabor, G. 1995, Monthly Notices of the Royal Astronomical Society, 276, 663
Böehringer, H., & Morfill, G. E. 1988, The Astrophysical Journal, 330, 609
Booth, C. M., & Schaye, J. 2009, MNRAS, 398, 53
Brüggen, M. 2003a, The Astrophysical Journal, 593, 700
—. 2003b, The Astrophysical Journal, 592, 839
Bryan, G. L., et al. 2014, The Astrophysical Journal Supplement Series, 211, 19
Butsky, I. S., & Quinn, T. R. 2018, The Astrophysical Journal, 868, 108
Cavagnolo, K. W., Donahue, M., Voit, G. M., & Sun, M. 2009, ApJS, 182, 12
Chandran, B. D. G., & Cowley, S. C. 1998, Physical Review Letters, 80, 3077
Ciotti, L., & Ostriker, J. P. 1997, The Astrophysical Journal, 487, L105
Colafrancesco, S., Dar, A., & De Rújula, A. 2004, Astronomy and Astrophysics, 413, 441
Dekel, A., & Birnboim, Y. 2007, Monthly Notices of the Royal Astronomical Society, 383, 119
—. 2008, MNRAS, 383, 119
Domainko, W., Gitti, M., Schindler, S., & Kapferer, W. 2004, Astronomy & Astrophysics, 425, L21
Dubois, Y., Devriendt, J., Slyz, A., & Teyssier, R. 2010, Monthly Notices of the Royal Astronomical Society, 409, 985
Fabian, A. C., Sanders, J. S., Taylor, G. B., Allen, S. W., Crawford, C. S., Johnstone, R. M., & Iwasawa, K. 2006, MNRAS, 366, 417
Fabian, A. C., et al. 2000, MNRAS, 318, L65
Fabjan, D., Borgani, S., Tornatore, L., Saro, A., Murante, G., & Dolag, K. 2010, Monthly Notices of the Royal Astronomical Society, 401, 1670
Gaspari, M. 2016, Galaxies at High Redshift and Their Evolution Over Cosmic Time, 319, 17
Gaspari, M., Brighenti, F., & Temi, P. 2012a, Monthly Notices of the Royal Astronomical Society, 424, 190
Gaspari, M., Melioli, C., Brighenti, F., & D'Ercole, A. 2011, Monthly Notices of the Royal Astronomical Society, 411, 349
Gaspari, M., Ruszkowski, M., & Sharma, P. 2012b, The Astrophysical Journal, 746, 94
Gaspari, M., & Sądowski, A. 2017, The Astrophysical Journal, 837, 149
Gaspari, M., Temi, P., & Brighenti, F. 2017, Monthly Notices of the Royal Astronomical Society, 466, 677
Gómez, P. L., Loken, C., Roettiger, K., & Burns, J. O. 2002, The Astrophysical Journal, 569, 122
Hahn, O., Martizzi, D., Wu, H.-Y., Evrard, A. E., Teyssier, R., & Wechsler, R. H. 2017, Monthly Notices of the Royal Astronomical Society, 470, 166
Hillel, S., & Soker, N. 2016, Monthly Notices of the Royal Astronomical Society, 455, 2139
Huarte-Espinosa, M., Frank, A., Blackman, E. G., Ciardi, A., Hartigan, P., Lebedev, S. V., & Chittenden, J. P. 2012, The Astrophysical Journal, 757, 66
Jubelgas, M., Springel, V., & Dolag, K. 2004, Monthly Notices of the Royal Astronomical Society, 351, 423
Jubelgas, M., Springel, V., Enßlin, T., & Pfrommer, C. 2008, Astronomy and Astrophysics, 481, 33
Khosroshahi, H. G., Jones, L. R., & Ponman, T. J. 2004, Monthly Notices of the Royal Astronomical Society, 349, 1240
Li, H., Lapenta, G., Finn, J. M., Li, S., & Colgate, S. A. 2006, The Astrophysical Journal, 643, 92
Li, Y., & Bryan, G. L. 2012, The Astrophysical Journal, 747, 26
—. 2014, The Astrophysical Journal, 789, 54
Li, Y., Bryan, G. L., Ruszkowski, M., Voit, G. M., O'Shea, B. W., & Donahue, M. 2015, ApJ, 811, 73
Loewenstein, M., Zweibel, E. G., & Begelman, M. C. 1991, The Astrophysical Journal, 377, 392
Malyshkin, L., & Kulsrud, R. 2001, The Astrophysical Journal, 549, 402
Markevitch, M., Vikhlinin, A., & Mazzotta, P. 2001, The Astrophysical Journal, 562, L153
Martizzi, D., Hahn, O., Wu, H.-Y., Evrard, A. E., Teyssier, R., & Wechsler, R. H. 2016, Monthly Notices of the Royal Astronomical Society, 459, 4408
McDonald, M., Veilleux, S., Rupke, D. S. N., & Mushotzky, R. 2010, ApJ, 721, 1262
McDonald, M., et al. 2019, The Astrophysical Journal, 885, 63
McNamara, B. R., & Nulsen, P. E. J. 2007, Annual Review of Astronomy and Astrophysics, 45, 117
McNamara, B. R., et al. 2000, ApJL, 534, L135
Meece, G. R., O'Shea, B. W., & Voit, G. M. 2015, The Astrophysical Journal, 808, 43
Meece, G. R., Voit, G. M., & O'Shea, B. W. 2017, The Astrophysical Journal, 841, 17pp
Meece Jr, G. R. 2016, AGN feedback and delivery methods for simulations of cool-core galaxy clusters (Michigan State University)
Nakamura, M., Li, H., & Li, S. 2006, The Astrophysical Journal, 652, 1059
—. 2007, The Astrophysical Journal, 656, 721
Narayan, R., & Medvedev, M. V. 2001, The Astrophysical Journal, 562, L129
Navarro, J. F., Frenk, C. S., & White, S. D. M. 1997, ApJ, 490, 493
Nelson, D., et al. 2019, Monthly Notices of the Royal Astronomical Society, 490, 3234
Panagoulia, E. K., Fabian, A. C., & Sanders, J. S. 2014, Monthly Notices of the Royal Astronomical Society, 438, 2341
Pfrommer, C., Enßlin, T. A., Springel, V., Jubelgas, M., & Dolag, K. 2007, Monthly Notices of the Royal Astronomical Society, 378, 385
Prasad, D., Sharma, P., & Babul, A. 2015, ApJ, 811, 108
—. 2017, Monthly Notices of the Royal Astronomical Society, 471, 1531

—. 2018, The Astrophysical Journal, 863, 62
Pratt, G. W., Croston, J. H., Arnaud, M., & Böhringer, H. 2009, Astronomy and Astrophysics, 498, 361
Rephaeli, Y., & Silk, J. 1995, The Astrophysical Journal, 442, 91
Revaz, Y., Combes, F., & Salomé, P. 2008, A&A, 477, L33
Ritchie, B. W., & Thomas, P. A. 2002, Monthly Notices of the Royal Astronomical Society, 329, 675
Roettiger, K., Loken, C., & Burns, J. O. 1997, The Astrophysical Journal Supplement Series, 109, 307
Russell, H. R., et al. 2016, MNRAS, 458, 3134
—. 2017, ApJ, 836, 130
Ruszkowski, M., Brüggen, M., & Begelman, M. C. 2004, The Astrophysical Journal, 611, 158
Ruszkowski, M., & Oh, S. P. 2011, Monthly Notices of the Royal Astronomical Society, 414, 1493
Schure, K. M., Kosenko, D., Kaastra, J. S., Keppens, R., & Vink, J. 2009, Astronomy & Astrophysics, 508, 751, arXiv: 0909.5204
Short, C. J., Thomas, P. A., & Young, O. E. 2013, Monthly Notices of the Royal Astronomical Society, 428, 1225, arXiv: 1201.1104
Sijacki, D., Springel, V., Di Matteo, T., & Hernquist, L. 2007, Monthly Notices of the Royal Astronomical Society, 380, 877
Smith, B., O'Shea, B. W., Voit, G. M., Ventimiglia, D., & Skillman, S. W. 2013, ApJ, 778, 152
Stone, J. M., & Norman, M. L. 1992, The Astrophysical Journal Supplement Series, 80, 753
Tabor, G., & Binney, J. 1993, Monthly Notices of the Royal Astronomical Society, 263, 323
Teyssier, R. 2002, Astronomy & Astrophysics, 385, 337
Tremmel, M., Karcher, M., Governato, F., Volonteri, M., Quinn, T. R., Pontzen, A., Anderson, L., & Bellovary, J. 2017, Monthly Notices of the Royal Astronomical Society, 470, 1121
Tremmel, M., et al. 2019, Monthly Notices of the Royal Astronomical Society, 483, 3336, arXiv: 1806.01282
Turk, M. J., Smith, B. D., Oishi, J. S., Skory, S., Skillman, S. W., Abel, T., & Norman, M. L. 2011, The Astrophysical Journal Supplement Series, 192, 9
Voigt, L. M., Schmidt, R. W., Fabian, A. C., Allen, S. W., & Johnstone, R. M. 2002, Monthly Notices of the Royal Astronomical Society, 335, L7
Voit, G. M., & Bryan, G. L. 2001, Nature, 414, 425
Voit, G. M., Meece, G., Li, Y., O'Shea, B. W., Bryan, G. L., & Donahue, M. 2017, The Astrophysical Journal, 845, 80
Weinberger, R., et al. 2017, Monthly Notices of the Royal Astronomical Society, 465, 3291
Wu, H.-Y., Evrard, A. E., Hahn, O., Martizzi, D., Teyssier, R., & Wechsler, R. H. 2015, Monthly Notices of the Royal Astronomical Society, 452, 1982
Wu, K. K. S., Fabian, A. C., & Nulsen, P. E. J. 1998, Monthly Notices of the Royal Astronomical Society, 301, L20
Yang, H.-Y. K., & Reynolds, C. S. 2016, \apj, 829, 90
Zhuravleva, I., et al. 2014, Nature, 515, 85
ZuHone, J. A., Markevitch, M., & Johnson, R. E. 2010, The Astrophysical Journal, 717, 908